

Nonequilibrium orbital transitions via applied electrical current in calcium ruthenatesHengdi Zhao,¹ Bing Hu,^{1,2} Feng Ye,^{3,*} Christina Hoffmann,³ Itamar Kimchi,^{1,4,†} and Gang Cao^{1,‡}¹*Department of Physics, University of Colorado, Boulder, Colorado 80309, USA*²*School of Mathematics and Physics, North China Electric Power University, Beijing 102206, China*³*Neutron Scattering Division, Oak Ridge National Laboratory, Oak Ridge, Tennessee 37831, USA*⁴*JILA, NIST and Department of Physics, University of Colorado, Boulder, Colorado 80309, USA*

(Received 22 August 2019; published 11 December 2019)

Simultaneous control of structural and physical properties via applied electrical current poses a new, key research topic with both fundamental and technological significance. Studying the spin-orbit-coupled antiferromagnet Ca_2RuO_4 , and its derivative with 3% Mn doping to alleviate the violent first-order transition at 357 K, we find that a small applied electrical current couples to the lattice by significantly reducing its orthorhombic distortions and octahedral rotations, while concurrently diminishing the 125-K antiferromagnetic transition. Further increasing electrical current density above 0.15 A/cm^2 induces a new nonequilibrium orbital state, with a transition signature at 80 K that features a simultaneous jump in both magnetization and electrical resistivity, sharply contrasting the current-free state. We argue that nonequilibrium electron occupancies of the t_{2g} orbitals stabilized by applied current drive the observed lattice changes and thereby the novel phenomena in this system. Finally, we note that current-induced diamagnetism reported in recent literature [C. Sow *et al.*, *Science* **358**, 1084 (2017).] is not discerned in either slightly doped or pure Ca_2RuO_4 .

DOI: [10.1103/PhysRevB.100.241104](https://doi.org/10.1103/PhysRevB.100.241104)

$4d/5d$ -electron-based oxides with inherent strong spin-orbit interactions and significant electronic correlations create an entirely new hierarchy of energy scales and unique competitions between fundamental interactions. As a result, exotic quantum states arise whenever competing interactions conspire to generate large susceptibilities to small, external stimuli [1].

The antiferromagnetic (AFM) insulator Ca_2RuO_4 is a good example [2,3]. With $\text{Ru}^{4+}(4d^4)$ ions, it exhibits a metal-insulator transition at $T_{\text{MI}} = 357 \text{ K}$ [4], which marks a concomitant and particularly violent structural transition with a severe rotation and tilting of RuO_6 . This structural transition removes the t_{2g} orbital degeneracy (d_{xy}, d_{yz}, d_{zx}), dictating physical properties of Ca_2RuO_4 [4–15]. An AFM transition occurs only at a considerably lower Néel temperature $T_N = 110 \text{ K}$ [2,3], highlighting its close association with a further distorted structure. Extensive investigations of this system have established that quantum effects are intimately coupled to lattice perturbations [7,12–19].

An early study demonstrates that electronic properties of Ca_2RuO_4 are sensitive to applied electrical current [20]. More recent investigations report current-induced diamagnetism [21] and current-induced nonequilibrium state [22]. It has become increasingly clear that electrical current as a new stimulus/probe controls quantum states in an unprecedented fashion. This is certainly manifested in our earlier study that demonstrates simultaneous current control of structural and physical properties in the spin-orbit-coupled Sr_2IrO_4 [23].

In this work, we investigate structural, magnetic, and transport properties as a function of electrical current and temperature in 3% Mn-doped Ca_2RuO_4 , and, for comparison, in pure Ca_2RuO_4 and 9% Mn-doped Ca_2RuO_4 . It is emphasized that the dilute Mn doping for Ru preserves the essential structural and physical properties of Ca_2RuO_4 but weakens the often pulverizing first-order structural phase transition at 357 K, making the single crystals more robust to sustain thermal cycling needed for thorough measurements [18,19]. This work reveals that a coupling between *small* applied electrical current and the lattice drastically reduces the orthorhombic distortion and the octahedral rotation. The current-reduced lattice distortions in turn precipitously suppress the native AFM state and subsequently induce a nonequilibrium orbital state below 80 K that features a concurrent increase in both magnetization and electrical resistivity. The simultaneous measurements of both neutron diffraction and electrical resistivity provide a direct correlation between the current-reduced orthorhombicity and electrical resistivity. A temperature-current-density phase diagram generated based on the data illustrates a critical regime near a small current density, J , of 0.15 A/cm^2 that separates the native, diminishing AFM state and the emergent state. We argue that nonequilibrium electron occupancies of the t_{2g} orbitals stabilized by applied current drive the critical lattice changes, thus the novel phenomena in this correlated, spin-orbit-coupled system. This study also emphasizes the conspicuous absence of current-induced diamagnetism, which is reported to exist in Ca_2RuO_4 [21]. Detailed experimental techniques are presented in the Supplemental Material (SM) [24] along with Refs. [23,25–29]. We proceed with the discussion below focusing on current-induced changes in the magnetization, electrical resistivity, and then the lattice modifications.

*yef1@ornl.gov

†ikimchi@gmail.com

‡Corresponding author: gang.cao@colorado.edu

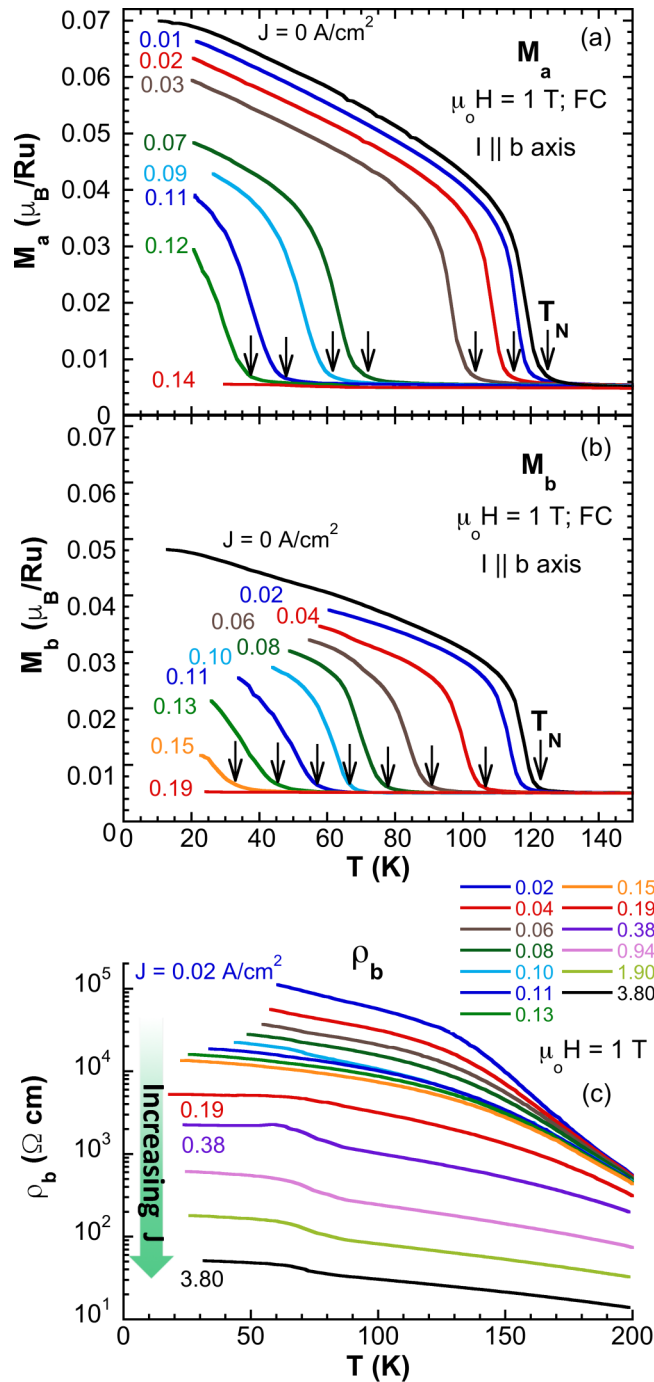


FIG. 1. Current-driven magnetic and transport properties of $\text{Ca}_2\text{Ru}_{0.97}\text{Mn}_{0.03}\text{O}_4$. The temperature dependence at various J applied along the b axis of (a) the a -axis magnetization M_a , (b) the b -axis magnetization M_b , and (c) the b -axis resistivity ρ_b . The magnetic field is at 1 T.

The magnetization along the a and b axes, M_a and M_b , sensitively responds to applied current along the b axis. As demonstrated in Figs. 1(a) and 1(b), the Néel temperature T_N decreases systematically and rapidly from 125 K at current density $J = 0 \text{ A/cm}^2$ to 29 K at $J = 0.15 \text{ A/cm}^2$ in M_b and 40 K at $J = 0.12 \text{ A/cm}^2$ in M_a and eventually vanishes at a critical current density $J_C \sim 0.15 \text{ A/cm}^2$ (the slight

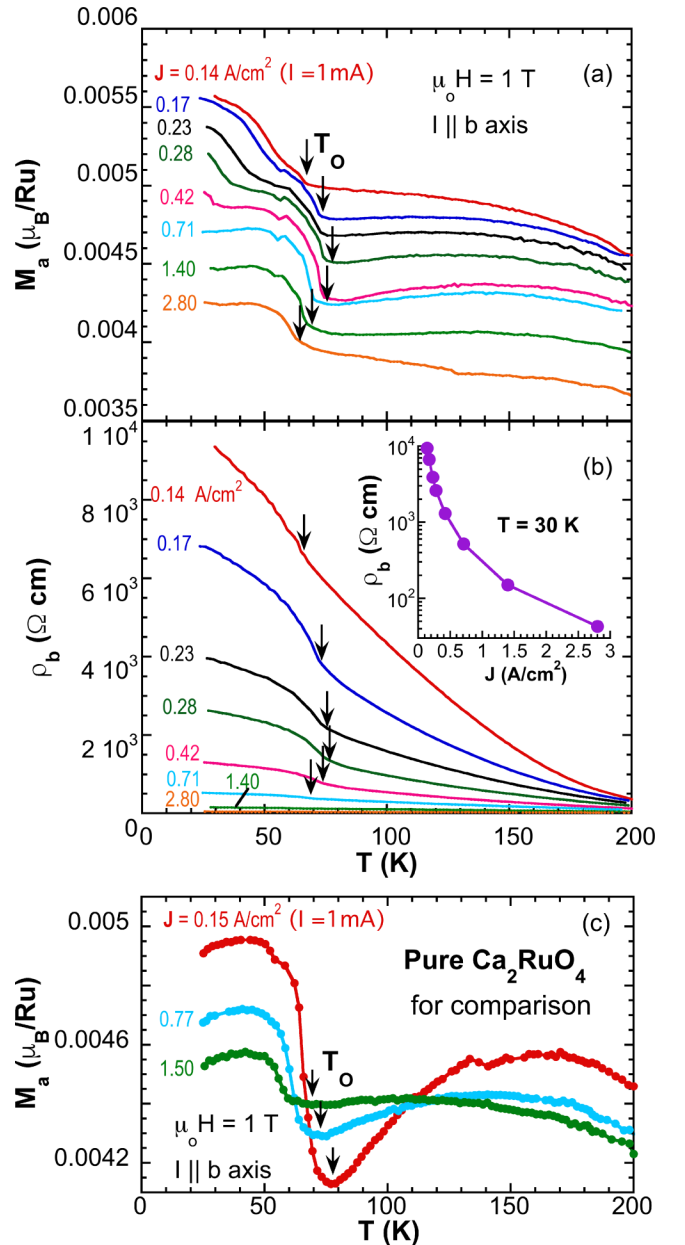


FIG. 2. Current-induced ordered state at $J \geq 0.14 \text{ A/cm}^2$. The temperature dependence at various J applied along the b axis of (a) M_a at 1 Tesla and (b) ρ_b for $\text{Ca}_2\text{Ru}_{0.97}\text{Mn}_{0.03}\text{O}_4$. Inset: ρ_b at 30 K as a function of J . (c) M_a at 1 Tesla for pure Ca_2RuO_4 at a few representative J for comparison.

difference in J_C for M_a and M_b is insignificant). The magnetic anisotropy between M_a and M_b with $M_a > M_b$ is evident in Figs. 1(a) and 1(b). Importantly, the diminishing AFM state is accompanied by a drastic decrease in the b -axis resistivity, ρ_b , by up to four orders of magnitude [Fig. 1(c)], consistent with concurrent changes in orbital populations dictating the transport properties [7–15]. Note that ρ_b and M_b are simultaneously measured.

A new, distinct phase emerges as the AFM state vanishes. Let us focus on M_a at higher J as M_b behaves similarly. Immediately following the disappearance of the AFM, a pronounced anomaly marked by T_O precipitates near J_C (see

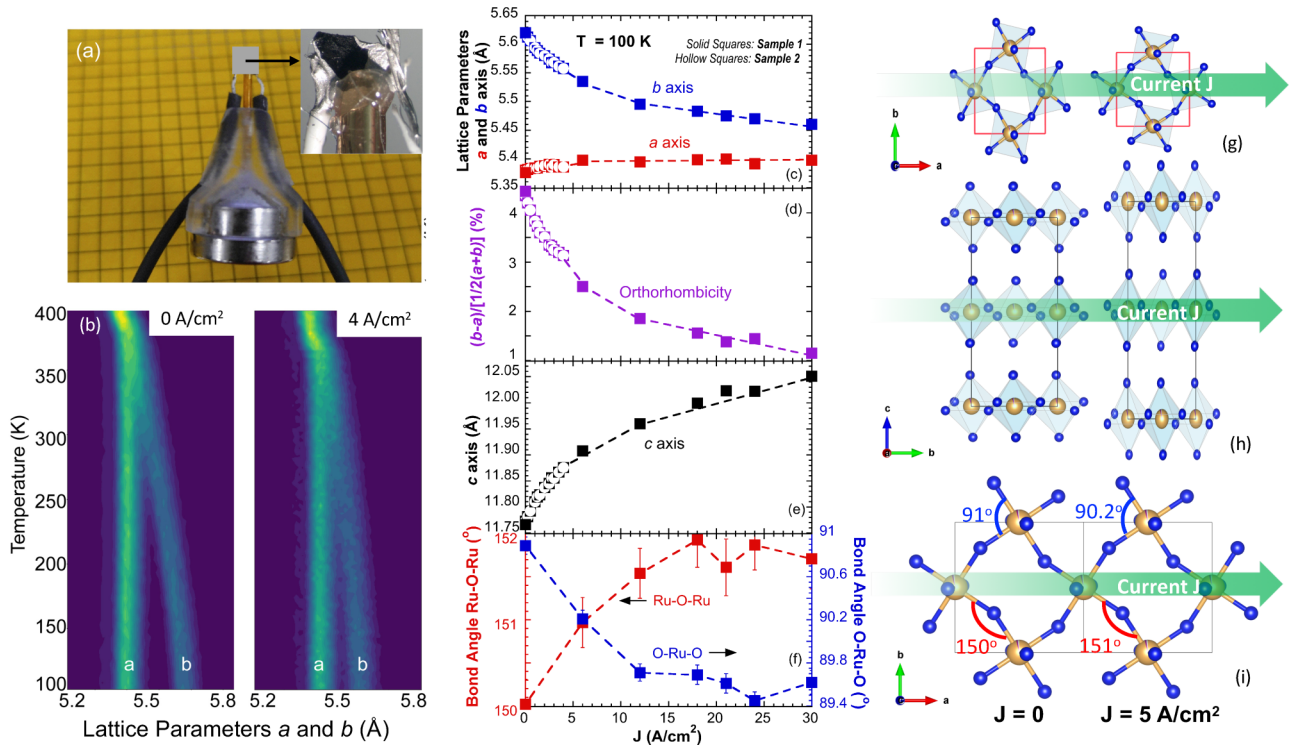


FIG. 3. The neutron diffraction and current-driven lattice changes in $\text{Ca}_2\text{Ru}_{0.97}\text{Mn}_{0.03}\text{O}_4$. (a) The sample holder for neutron diffraction with applied current. Inset: The single-crystal $\text{Ca}_2\text{Ru}_{0.93}\text{Mn}_{0.03}\text{O}_4$ with the electrical leads for applied current. (b) Two representative contour plots for the temperature dependence of the lattice parameters a , and b axis at current density $J = 0$ and 4 A/cm^2 applied in the basal plane. Note that the orthorhombicity is significantly reduced with increasing J . The current density J dependence at 100 K of (c) the a and b axes, (d) the orthorhombicity defined by $(b-a)/[(a+b)/2]$, (e) the c axis, and (f) the bond angles Ru-O-Ru (red, left scale) and O-Ru-O (blue, right scale). The schematics illustrating the current-induced lattice changes: (g) the reduced orthorhombicity, (h) the elongated unit cell, and (i) the increased bond angles; the displayed values for $J = 0$ and $J = 5 \text{ A/cm}^2$, respectively.

Fig. 2). The new transition temperature T_O rises initially, and peaks near $J = 0.28 \text{ A/cm}^2$ before slowly decreasing with increasing J [Fig. 2(a)]. The simultaneously measured ρ_b closely tracks M_a with a well-defined anomaly corresponding to T_O , signaling a strong correlation between electron transport and magnetization in this emergent state [Fig. 2(b)]. The concurrent change in both ρ_b and M_a at T_O sharply contrasts that of the native state in which $T_{\text{MI}} \gg T_N$ [4] and indicates the presence of a new type of state where magnetic response involves spin or orbital features or both.

The simultaneous rise in both M_a and ρ_b at T_O would suggest a possible Slater transition to a new AFM state. However, this is inconsistent with other experimental observations. First, a sample history dependence above T_O is seen in magnetization at higher current densities ($J > 1 \text{ A/cm}^2$) [30]. Although the transition at T_O is robust (no history dependence below T_O), a lack of history resetting above T_O even after hours or days of equilibration time [30] implies that the transition at T_O must involve changes not only in spins but also in orbital occupancies. Second, the disproportionately larger change in ρ_b below T_O , compared to that in M_a , also indicates that spins alone cannot account for such a change in ρ_b [Figs. 2(a) and 2(b)]. For example, ρ_b reduces by over three orders of magnitude below T_O as J increases from 0.14 to 2.8 A/cm^2 at 30 K [Fig. 2(b) inset] whereas M_b changes merely $\sim 10\%$ for the same J interval. All this contradicts a spin-driven Slater transition. Instead, it is consistent that the strong current

produces a nonequilibrium state with inhomogeneous orbital occupancies. Such a current-induced state does not coexist with the native AFM state, implying an incompatible nature of the new state with the equilibrium, native state. Such an incompatibility is also true for other magnetic materials currently under investigation [30].

It is striking that current-induced diamagnetism, which is reported to exist in pure Ca_2RuO_4 [21], is absent in not only $\text{Ca}_2\text{Ru}_{0.97}\text{Mn}_{0.03}\text{O}_4$ but also in pure Ca_2RuO_4 . For comparison and clarification, we conduct the same measurements on pure Ca_2RuO_4 and 9% Mn-doped Ca_2RuO_4 . M_a (and ρ_b , not shown) for pure Ca_2RuO_4 [Fig. 2(c)] and 9% Mn-doped Ca_2RuO_4 (SM, Fig. 5 [24]) exhibits behavior remarkably similar to that seen in Fig. 2(a) for 3% Mn-doped Ca_2RuO_4 . These results indicate the current-induced behavior above and below T_O arises from the underlying properties of Ca_2RuO_4 , independent of Mn doping. This is consistent with the fact that low Mn doping retains the underlying properties of Ca_2RuO_4 [19]. We also conduct a controlled study on the antiferromagnetic BaRuO_3 [25] whose magnetization has the same orders of magnitude; the results show no discernible current-induced changes in magnetization (SM Fig. 3 [24]), ruling out any possible spurious behavior from our experimental setup.

We now turn to the current-driven crystal structure. $\text{Ca}_2\text{Ru}_{0.97}\text{Mn}_{0.03}\text{O}_4$ preserves the orthorhombic distortions ($Pbca$, No. 61) of Ca_2RuO_4 [19]. The single crystal used for neutron diffraction with *in-plane* current applied is shown in

Fig. 3(a). Two representative contour plots for the temperature dependence of the lattice parameters a and b at current density $J = 0$ and 4 A/cm^2 [Fig. 3(b)] illustrate an abrupt change in the lattice parameters at T_{MI} but no discernible structural inhomogeneity, which would lead to a broadening of Bragg peaks. (Note that this is different from nonequilibrium or inhomogeneous orbital occupancies discussed above.) Moreover, Fig. 3(b) clearly shows a diminishing difference between the a and b axes or orthorhombicity with increasing J . Here we focus on the structural data at 100 K culled via neutron diffraction as a function of current density J applied within the basal plane. As shown in Fig. 3(c), one major effect is that the applied current progressively reduces the orthorhombicity, defined by $(b - a)/[(a + b)/2]$, from 4.4% at $J = 0 \text{ A/cm}^2$ to 2.5% at $J = 5 \text{ A/cm}^2$ and eventually to 1.2% at $J = 30 \text{ A/cm}^2$ [Fig. 3(d)]. At the same time, the c axis expands by 1.2% and 2.4% at $J = 5$ and 30 A/cm^2 , respectively [Fig. 3(e)]. Interestingly, the current-driven lattice changes are remarkably similar to those due to modest pressure ($< 2 \text{ GPa}$) [6]. The bond angle Ru-O-Ru, which defines the rotation of RuO_6 octahedra, increases by one degree at $J = 5 \text{ A/cm}^2$ and two degrees at $J = 18 \text{ A/cm}^2$, resulting in less buckled RuO_6 octahedra [Fig. 3(f)]. In addition, the bond angle O-Ru-O decreases from 91° to 90.2° at $J = 5 \text{ A/cm}^2$, close to the ideal 90° [Fig. 3(f)]. Remarkably, the lattice changes more rapidly at smaller J ($< 5 \text{ A/cm}^2$) than at larger J . In short, applied current significantly reduces the orthorhombic distortion from the tetragonal symmetry, expands the c axis, and relaxes the bond angles, as schematically illustrated in Figs. 3(g)–3(i).

A direct link between the current-reduced orthorhombicity and electrical resistivity is further revealed in Fig. 4. The contour plot of the orthorhombicity as functions of temperature and current density ranging from 0 to 4 A/cm^2 in Fig. 4(a) shows that the crystal structure sensitively responds to even a small current density J ($< 1 \text{ A/cm}^2$). Particularly, the orthorhombicity is significantly reduced with increasing J throughout the measured temperature range. This change almost perfectly traces that of the electrical resistivity that was simultaneously measured during the neutron diffraction measurements, as illustrated in Fig. 4(b). This comparison provides an explicit correlation between the current-driven lattice and transport properties. The applied current reduces the orthorhombicity, modifying the t_{2g} orbital occupancies that favor electron hopping. (Note that the structural transition at T_{MI} [blue area in Fig. 4(a)] barely shifts with J , confirming insignificant heating effect.)

Indeed, the more metallic state is a current-driven instability of an insulating state that is captured by local orbital occupancies. The experimental feature to explain is that applied in-plane current, as it suppresses T_N , also suppresses the transition to the insulator and the octahedral tilt and rotation while reducing the orthorhombicity and elongating the c axis [Figs. 3 and 4(a)–4(c)]. We now proceed to construct a theoretical framework that captures this feature through local orbital occupancies and overlaps. Without applied current, Ru^{4+} ions nominally have two holes in the t_{2g} orbitals but x-ray spectroscopy studies [1] suggest that a $1/2$ hole is transferred to the oxygen. At high temperatures, in the metallic state, the remaining $3/2$ hole is equally split in a 1:1 ratio between the d_{xy} orbital and the manifold of d_{xz}/d_{yz} orbitals

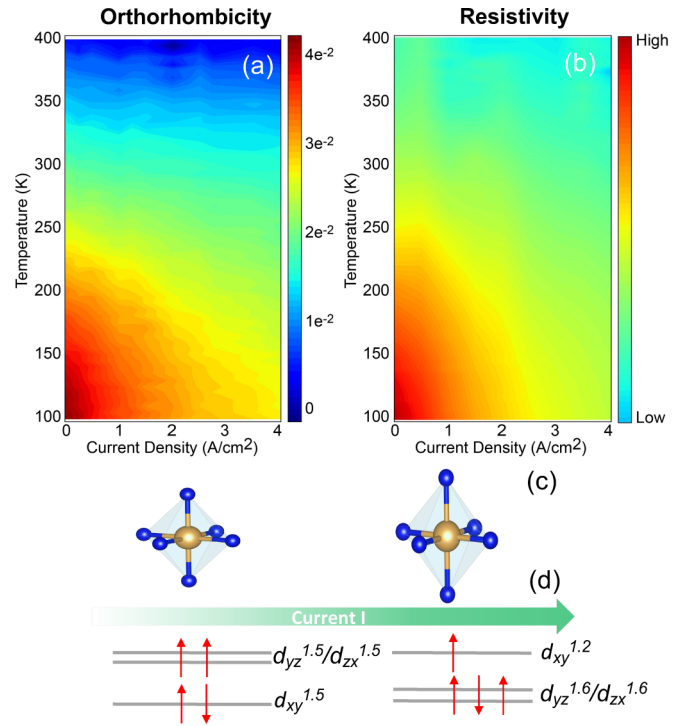


FIG. 4. Direct correlation between the orthorhombicity and the electrical resistivity of $\text{Ca}_2\text{Ru}_{0.97}\text{Mn}_{0.03}\text{O}_4$. The temperature-current-density contour plots for (a) the orthorhombicity and (b) electrical resistivity. The schematics illustrating at $T > T_O$ (c) the current-driven elongation of RuO_6 and (d) corresponding changes in t_{2g} orbital populations.

(giving an electron occupancy roughly $\sim d_{xy}^{1.2} d_{xz}^{1.6} d_{yz}^{1.6}$). At $T < T_{\text{MI}}$, the first-order structural transition at $T_{\text{MI}} = 357 \text{ K}$ leads to the lattice distortions and the rotation, tilting and flattening of RuO_6 , which transfers more holes from d_{xy} to d_{xz}/d_{yz} , leading to a 1:2 ratio of hole occupancies in d_{xy} vs d_{xz}/d_{yz} (giving an electron occupancy roughly $\sim d_{xy}^{1.5} d_{xz}^{1.5} d_{yz}^{1.5}$) [1]. The insulating state below T_{MI} thus has each orbital at exactly $3/4$ electron filling (or $1/4$ hole filling). In contrast, the metallic state above T_{MI} has unequal filling, with a nearly filled d_{xz}/d_{yz} manifold (fewer holes) and, importantly, a nearly half-filled d_{xy} orbital (more holes) [right sketch in Fig. 4(d)]. This analysis suggests that the conductivity in the metallic phase above T_{MI} [11] is primarily enhanced by the d_{xy} orbitals.

Now consider the nonequilibrium electron occupancies stabilized with an applied electric current. Within the d_{xy} band, the electrons have large hopping amplitude from each Ru ion to each of its four neighbors, via the p_x and p_y orbitals on the four surrounding oxygens. This is not true for the d_{xz} or d_{yz} bands. So half-filling the d_{xy} band is far more favorable for the conductivity than half-filling either the d_{xz} or d_{yz} bands or uniformly quarter-filling the entire multiband manifold.

Driving an in-plane current forces a metallic state to persist which, based on this picture, should lead to two effects: (1) the applied current minimizes crystalline distortions in the basal plane, so as to maximize interorbital hopping for in-plane conductivity; and (2) applying a current keeps the d_{xy} band as close to half-filling as possible, hence also avoiding the

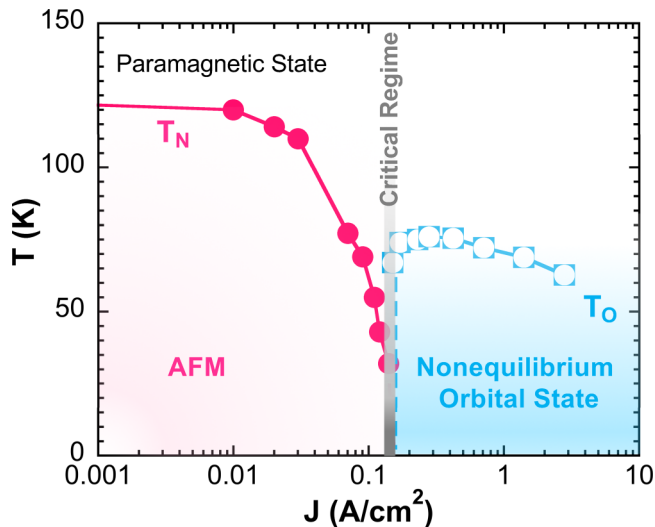


FIG. 5. (a) The T - J phase diagram illustrates that the applied current drives the system from the native AFM state (purple) through the critical regime near 0.15 A/cm^2 (gray) to the current-induced, nonequilibrium orbital state (blue).

crystal distortions that are known (from the metal-insulator transition at zero applied current) to force d_{xy} away from half-filling. These two effects [Figs. 4(b) and 4(c)] capture the experimentally observed behavior of the resistivity and crystal structure with applied current while T_N is suppressed. These

current-induced lattice changes then also explain the vanishing native AFM state with increasing J because the AFM state requires a combination of rotation, tilt, and flattening of RuO_6 octahedra hosting localized electrons [7,10,11], all of which are significantly weakened by applied current.

A temperature-current-density phase diagram generated based on the data presented above illustrates the diminishing AFM and the emergent, nonequilibrium order state characterized by T_O with increasing J , as shown in Fig. 5. The critical regime near $J_C = 0.15 \text{ A/cm}^2$ separates the two states and hosts a nonmagnetic state that is stabilized by delicate lattice changes discussed above. A spin-orbit-driven singlet $J_{\text{eff}} = 0$ state [31] is suggested but more fine-tuning of the lattice in this regime is needed to rule in or out this possibility. For $J > J_C$, current-induced inhomogeneous orbital occupancies may play a more dominant role dictating physical properties both above and below T_O . All in all, at the heart of the new phenomena are the critical lattice modifications via current-driven nonequilibrium electron populations of the t_{2g} orbitals.

This work is supported by NSF via Grants No. DMR 1712101 and No. DMR 1903888. Work at ORNL was sponsored by the Scientific User Facilities Division, Basic Energy Sciences, US Department of Energy (DOE). I.K. was supported by a National Research Council Fellowship through the National Institute of Standards and Technology. We thank Dr. Daniel Khomskii for useful discussions.

- [1] *Frontiers of 4D- and 5D-Transition Metal Oxides*, edited by G. Cao and L. E. De Long (World Scientific, Singapore, 2013).
- [2] G. Cao, S. McCall, M. Shepard, J. E. Crow, and R. P. Guertin, Magnetic and transport properties of single-crystal Ca_2RuO_4 : Relationship to superconducting Sr_2RuO_4 *Phys. Rev. B* **56**, R2916 (1997).
- [3] S. Nakatsuji, S. Ikeda, and Y. Maeno, Ca_2RuO_4 : New mott insulators of layered ruthenate, *J. Phys. Soc. Jpn.* **66**, 1868 (1997).
- [4] C. S. Alexander, G. Cao, V. Dobrosavljevic, S. McCall, J. E. Crow, E. Lochner, and R. P. Guertin, Destruction of the Mott insulating ground state of Ca_2RuO_4 by a structural transition, *Phys. Rev. B* **60**, R8422(R) (1999).
- [5] M. Braden, G. André, S. Nakatsuji, and Y. Maeno, Crystal and magnetic structure of Ca_2RuO_4 : Magnetoelastic coupling and the metal-insulator transition, *Phys. Rev. B* **58**, 847 (1998).
- [6] P. Steffens, O. Friedt, P. Alireza, W. G. Marshall, W. Schmidt, F. Nakamura, S. Nakatsuji, Y. Maeno, R. Lengsdorf, M. M. Abd-Elmeguid, and M. Braden, High-pressure diffraction studies on Ca_2RuO_4 , *Phys. Rev. B* **72**, 094104 (2005).
- [7] Z. Fang and K. Terakura, Magnetic phase diagram of $\text{Ca}_{2-x}\text{Sr}_x\text{RuO}_4$ governed by structural distortions, *Phys. Rev. B* **64**, 020509(R) (2001).
- [8] T. Hotta and E. Dagotto, Prediction of Orbital Ordering in Single-Layered Ruthenates, *Phys. Rev. Lett.* **88**, 017201 (2001).
- [9] J. S. Lee, Y. S. Lee, T. W. Noh, S.-J. Oh, Jaejun Yu, S. Nakatsuji, H. Fukazawa, and Y. Maeno, Electron and Orbital Correlations in $\text{Ca}_{2-x}\text{Sr}_x\text{RuO}_4$ Probed by Optical Spectroscopy, *Phys. Rev. Lett.* **89**, 257402 (2002).
- [10] J. H. Jung, Z. Fang, J. P. He, Y. Kaneko, Y. Okimoto, and Y. Tokura, Change of Electronic Structure in Ca_2RuO_4 Induced by Orbital Ordering, *Phys. Rev. Lett.* **91**, 056403 (2003).
- [11] E. Gorelov, M. Karolak, T. O. Wehling, F. Lechermann, A. I. Lichtenstein, and E. Pavarini, Nature of the Mott Transition in Ca_2RuO_4 , *Phys. Rev. Lett.* **104**, 226401 (2010).
- [12] G.-Q. Liu, Spin-orbit coupling induced Mott transition in $\text{Ca}_{2-x}\text{Sr}_x\text{RuO}_4$ ($0 \leq x \leq 0.2$), *Phys. Rev. B* **84**, 235136 (2011).
- [13] G. Cao, S. McCall, V. Dobrosavljevic, C. S. Alexander, J. E. Crow, and R. P. Guertin, Ground-state instability of the Mott insulator Ca_2RuO_4 : Impact of slight La doping on the metal-insulator transition and magnetic ordering, *Phys. Rev. B* **61**, R5053(R) (2000).
- [14] F. Nakamura, T. Goko, M. Ito, T. Fujita, S. Nakatsuji, H. Fukazawa, Y. Maeno, P. Alireza, D. Forsythe, and S. R. Julian, From Mott insulator to ferromagnetic metal: A pressure study of Ca_2RuO_4 , *Phys. Rev. B* **65**, 220402(R) (2002).
- [15] I. Zegkinoglou, J. Stremper, C. S. Nelson, J. P. Hill, J. Chakhalian, C. Bernhard, J. C. Lang, G. Srajer, H. Fukazawa, S. Nakatsuji, Y. Maeno, and B. Keimer, Orbital Ordering Transition in Ca_2RuO_4 Observed with Resonant X-Ray Diffraction, *Phys. Rev. Lett.* **95**, 136401 (2005).
- [16] S. Nakatsuji and Y. Maeno, Quasi-Two-Dimensional Mott Transition System $\text{Ca}_{2-x}\text{Sr}_x\text{RuO}_4$, *Phys. Rev. Lett.* **84**, 2666 (2000).
- [17] C. S. Snow, S. L. Cooper, G. Cao, J. E. Crow, H. Fukazawa, S. Nakatsuji, and Y. Maeno, Pressure-Tuned Collapse of the Mott-Like State in $\text{Ca}_{n+1}\text{Ru}_n\text{O}_{3n+1}$ ($n = 1, 2$): Raman Spectroscopic Studies, *Phys. Rev. Lett.* **89**, 226401 (2002).
- [18] T. F. Qi, O. B. Korneta, S. Parkin, L. E. DeLong, P. Schlottmann, and G. Cao, Negative Volume Thermal Expansion Via Orbital

- and Magnetic Orders in $\text{Ca}_2\text{Ru}_{1-x}\text{Cr}_x\text{O}_4$ ($0 < x < 0.13$), *Phys. Rev. Lett.* **105**, 177203 (2010).
- [19] T. F. Qi, O. B. Korneta, S. Parkin, J. Hu, and G. Cao, Magnetic and orbital orders coupled to negative thermal expansion in Mott insulators $\text{Ca}_2\text{Ru}_{1-x}\text{M}_x\text{O}_4$ ($M = \text{Mn}$ and Fe), *Phys. Rev. B* **85**, 165143 (2012).
- [20] R. Okazaki, Y. Nishina, Y. Yasui, F. Nakamura, T. Suzuki, and I. Terasaki, Current-induced gap suppression in the mott insulator Ca_2RuO_4 , *J. Phys. Soc. Jpn.* **82**, 103702 (2013).
- [21] C. Sow, S. Yonezawa, S. Kitamura, T. Oka, K. Kuroki, F. Nakamura, and Y. Maeno, Current-induced strong diamagnetism in the Mott insulator Ca_2RuO_4 , *Science* **358**, 1084 (2017).
- [22] J. Bertinshaw, N. Gurung, P. Jorba, H. Liu, I. M. Schmid, D. T. Mantadakis, M. Daghofer, M. Krautloher, I. A. Jain, G. H. Ryu, O. Fabelo, P. Hansmann, G. Khaliullin, C. Peiderer, B. Keimer, and B. J. Kim, Unique Crystal Structure of Ca_2RuO_4 in the Current Stabilized Semimetallic State, *Phys. Rev. Lett.* **123**, 137204 (2019).
- [23] G. Cao, J. Terzic, H. D. Zhao, H. Zheng, L. E. De Long, and Peter S. Riseborough, Electrical Control of Structural and Physical Properties via Strong Spin-Orbit Interactions in Sr_2IrO_4 , *Phys. Rev. Lett.* **120**, 017201 (2018).
- [24] See Supplemental Material at <http://link.aps.org/supplemental/10.1103/PhysRevB.100.241104> for experimental details and additional data.
- [25] G. Cao, J. E. Crow, R. P. Guertin, P. Henning, C. C. Homes, M. Strongin, D. N. Basov, and E. Lochner, Charge density wave formation accompanying ferromagnetic ordering in quasi-one-dimensional BaIrO_3 , *Solid State Commun.* **113**, 657 (2000).
- [26] G. M. Sheldrick, A short history of SHELX, *Acta Crystallogr., Sect. A: Found. Adv.* **64**, 112 (2008).
- [27] J. Zikovsky, Peter F. Peterson, X. P. Wang, M. Frost, and C. Hoffmann, CrystalPlan: an experiment-planning tool for crystallography, *J. Appl. Crystallogr.* **44**, 418 (2011).
- [28] A. J. Schultz, M. R. V. Jørgensen, X. Wang, R. L. Mikkelsen, D. J. Mikkelsen, V. E. Lynch, P. F. Peterson, M. L. Green, and C. M. Hoffmann, Integration of neutron time-of-flight single-crystal Bragg peaks in reciprocal space, *J. Appl. Crystallogr.* **47**, 915 (2014).
- [29] A. J. Schultz, K. Srinivasan, R. G. Teller, J. M. Williams, and C. M. Lukehart, Single-crystal, time-of-flight, neutron-diffraction structure of hydrogen cis-diacetyltetracarbonylrhenate, $[\text{cis}-(\text{OC})_4\text{Re}(\text{CH}_3\text{CO})_2]\text{H}$: a metallaacetylacetonate molecule, *J. Am. Chem. Soc.* **106**, 999 (1984).
- [30] B. Hu, H. Zhao, and G. Cao (unpublished).
- [31] G. Khaliullin, Excitonic Magnetism in Van Vlecktype d^4 Mott Insulators *Phys. Rev. Lett.* **111**, 197201 (2013).